Hydrogen in layered iron arsenides: Indirect electron doping to induce superconductivity

Taku Hanna,[1] Yoshinori Muraba,[1] Satoru Matsuishi,[1] Naoki Igawa,[2] Katsuaki Kodama,[2] Shin-ichi Shamoto,[2] and Hideo Hosono[1,3,*]

[1]*Materials and Structures Laboratory, Tokyo Institute of Technology, 4259 Nagatsuta-cho, Midori-ku, Yokohama 226-8503, Japan*

[2]*Quantum Beam Science Directorate, Japan Atomic Energy Agency, Tokai, Ibaraki 319-1195, Japan*

[3]*Frontier Research Center, Tokyo Institute of Technology, 4259 Nagatsuta-cho, Midori-ku, Yokohama 226-8503, Japan*

(Received 17 February 2011; revised manuscript received 6 April 2011; published 15 June 2011)

Utilizing the high stability of calcium and rare-earth hydrides, $CaFeAsF_{1-x}H_x$ (x = 0.0–1.0) and $SmFeAsO_{1-x}H_x$ (x = 0.0–0.47) have been synthesized using high pressure to form hydrogen-substituted 1111-type iron-arsenide superconductors. Neutron diffraction and density functional calculations have demonstrated that the hydrogens are incorporated as H^- ions occupying F^- sites in the blocking layer of CaFeAsF. The resulting $CaFeAsF_{1-x}H_x$ is nonsuperconducting, whereas, $SmFeAsO_{1-x}H_x$ is a superconductor, with an optimal $T_c = 55$ K at $x \sim 0.2$. It was found that up to 40% of the O^{2-} ions can be replaced by H^- ions, with electrons being supplied into the FeAs layer to maintain neutrality ($O^{2-} = H^- + e^-$). When x exceeded 0.2, T_c was reduced corresponding to an electron overdoped region.

DOI: 10.1103/PhysRevB.84.024521 PACS number(s): 74.70.Xa, 74.62.Bf, 74.25.F–

I. INTRODUCTION

Since the discovery of superconductivity in $LaFeAsO_{1-x}F_x$ (T_c = 28 K),[1] layered iron pnictides and related materials have been intensively investigated as candidates for high-T_c superconductors. To date, various types of iron-based superconductors have been synthesized,[2–11] with the highest T_c of ∼ 55 K being recorded in $SmFeAsO_{0.9}F_{0.1}$.[12–17] The 1111-type iron arsenides LnFeAsO (Ln = lanthanide) with a ZrCuSiAs-type structure[18] are composed of stacks of alternating FeAs anti-fluorite-type conducting layers and LnO fluorite-type blocking layers. Although the parent compounds are nonsuperconducting at ambient pressures, they are superconducting when electrons are doped into the FeAs layer via fluorine substitution at the oxygen sites ($O^{2-} = F^- + e^-$),[1,13–17] oxygen vacancy formation ($O^{2-} = V_O + 2e^-$),[19–21] or transition-metal (TM, with excess electrons when compared with Fe, such as Co or Ni) substitution into the iron site.[22–25] TM substitution, adding electrons to the FeAs layer, is a direct doping mode, whereas, F-substitution or O-vacancy formation is an indirect mode because impurities are doped to the blocking layers and the electrons are transferred to the FeAs layers. The general consensus is that indirect doping gives a higher T_c because less structural and electrical disturbances occur in the superconducting layers. However, overdoping via the indirect mode has not been confirmed for most 1111-type iron arsenides. In other words, further improvement in the T_c may be possible. For example, the solubility limit of fluorine substitution in LnFeAsO is lower than 20%. This fact is in contrast to alkali-metal substitution in 122-type $Ba_{1-x}K_xFe_2As_2$ superconductors in which the Ba site can fully be replaced by K.[26] This restraint also makes it difficult to complete the electronic phase diagram (doping level vs critical temperatures) beyond the optimal doping level. Completion of the phase diagram is important not only to improve T_c, but also to understand superconductivity. Besides, although several papers have reported on the variation of T_c with nominal oxygen vacancy or hydrogen content in the 1111 system, the chemical states and the analyzed composition have not been clarified to date.[19,20,27–29] This ambiguity is an obstacle for understanding the emerging and carrier concentration dependence on T_c.

In this paper, we propose a method for indirect electron doping to induce superconductivity in 1111-type iron arsenides. By using a high-pressure synthesis method with an excess hydrogen source, CaFeAsH, an analog of LnFeAsO, and the solid solution between CaFeAsF[30,31] and CaFeAsH ($CaFeAsF_{1-x}H_x$ where $0 \leqslant x \leqslant 1$) have been synthesized. While $CaFeAsF_{1-x}H_x$ is nonsuperconducting like LnFeAsO, these results indicate the anion site in the blocking layer can be substituted with H^-. Considering the facile formation of metal hydrides with rare earths, H^- appears to be stabilized in these rare-earth compounds. Thus, the hydrogen substitution technique has been applied to electron doping in SmFeAsO as with fluorine substitution ($O^{2-} = H^- + e^-$). Up to 40% of the oxygen sites were replaced successfully by hydrogen ($SmFeAsO_{1-x}H_x$, $0 < x \leqslant 0.4$), and superconductivity with a maximum T_c = 55 K ($x \sim 0.2$) was induced. Above 20% hydrogen substitution, T_c was decreased, indicating that electron overdoping, which was not seen with F substitution in this system, was observed.[32–34]

II. EXPERIMENTAL

CaFeAsH was synthesized by the solid-state reaction of CaAs, Fe_2As, and CaH_2 with $LiAlH_4$ as an excess hydrogen source, at 1000°C and 2 GPa ($CaAs + Fe_2As + CaH_2 \rightarrow 2CaFeAsH$). A belt-type anvil cell was employed for the high-pressure synthesis. Powders of CaAs and Fe_2As were prepared from their respective metals (Ca: 99.99% Sigma-Aldrich, Fe: 99.9% Kojyundo Chemical Laboratory Co., Ltd., and As: 99.9999% Kojyundo Chemical Laboratory Co., Ltd.) and CaH_2/CaD_2 were synthesized by heating calcium metal in an H_2/D_2 atmosphere. The solid solution of fluoride and hydride, $CaFeAsF_{1-x}H_x$, was obtained over the full x range by adding CaF_2 to the starting mixture in the high-pressure synthesis, $CaAs + Fe_2As + (1-x)\,CaF_2 + x\,CaH_2 \rightarrow 2CaFeAsF_{1-x}H_x$. All starting materials and precursors for the synthesis were prepared in a glove box (Miwa Mfg. Co., Ltd.) filled with purified Ar gas (H_2O, O_2 < 1 ppm). The

mixture of starting materials was placed into a BN capsule. Following the internal hydrogen source technique developed by Fukai and Okuma,[35,36] $LiAlH_4$ (98%, Tokyo Kasei Kogyo Co., Ltd.) was also placed in the capsule with a BN separator as a supplementary hydrogen source. The deuterated analog, CaFeAsD, was also prepared using CaD_2 and $LiAlD_4$(90% CP, 98% D, Tokyo Kasei Kogyo Co., Ltd.). Like $CaFeAsF_{1-x}H_x$, $SmFeAsO_{1-x}H_x$ was prepared by the solid-state reactions of SmAs, FeAs, Fe_2As, Sm_2O_3, and SmH_2 at 2 GPa at 1200 °C; $(2+x)$ SmAs + $(2+x)$ Fe_2As + $(2-2x)$ FeAs + $(2-2x)$ Sm_2O_3 + $3x$ SmH_2 → $6SmFeAsO_{1-x}H_x$. SmAs and SmH_2 were prepared by the reaction of Sm metal with arsenic or hydrogen gas. In this case, a mixture of $NaBH_4$ and $Ca(OH)_2$ was used as the excess hydrogen source.

The resulting crystalline phases were identified by powder x-ray diffraction (XRD) using a Bruker AXS GmbH diffractometer model D8 ADVANCE (Cu-rotating anode). Rietveld analysis of XRD patterns was performed using the TOPAS code.[37] The amount of hydrogen incorporated in the resulting samples was evaluated by thermogravimetry and mass spectroscopy (TG-MS) performed using a Bruker AXS GmbH TG-DTA/MS9610 equipped with a gas feed port to inject the standard H_2 gas into the sample chamber. Twenty milligrams of sample were heated to 800 °C with a heating rate of 20 $Kmin^{-1}$ under a helium gas flow. Hydrogen released from the sample, in the form of an H_2 molecule was ionized and was detected by a quadrupole mass spectrometer as an ion with mass-to-charge ratio $(m/z) = 2$. Elemental composition of $SmFeAsO_{1-x}H_x$ (Sm:Fe:As:O) was determined by a JEOL, Inc. JXA-8530F electron-probe microanalyzer (EPMA) equipped with a field-emission-type electron gun and wavelength dispersive x-ray detectors. The micrometer-scale compositions within the main phase were probed on five to ten focal points, and the results were averaged.

Neutron powder diffraction (NPD) of CaFeAsD was measured on ∼3 g of sample by the high-resolution powder diffractometer installed at the JRR-3 reactor of the Japan Atomic Energy Agency (beam collimation of 30′–40′-(sample)-6′ with neutron wavelength $\lambda = 0.182\ 391$ nm). Rietveld analyses of the NPD patterns were performed using the RIETAN-FP code.[38]

The dc resistivity and magnetic susceptibility were measured in the temperature range of 2–300 K, using a physical properties measurement system (Quantum Design, Inc.) with a vibrating sample magnetometer attachment.

To investigate the electronic structure of CaFeAsH, density functional theory calculations were performed using the generalized gradient approximation Perdew-Burke-Ernzerhof functional[39] and the projected augmented plane-wave method[40] implemented in the Vienna *ab initio* simulation program (VASP) code,[41] following Refs. 42 and 43. A $\sqrt{2}a \times \sqrt{2}b \times \sqrt{2}c$ supercell containing eight chemical formulas was used for the calculation, and the plane-wave basis set cutoff was set to 600 eV. For Brillouin-zone integrations to calculate the total energy and density of states (DOS), 4 × 4 × 2 Monkhorst-Pack grids of k points were used. To obtain the projected DOS, the charge density was decomposed over the atom-centered spherical harmonics with a Wigner-Seitz radius $r = (3V_{cell}/4\pi N)^{1/3}$, where V_{cell} and N are the unit-cell volume and the number of atoms in a unit cell, respectively.

III. RESULTS AND DISCUSSION

Figure 1(a) shows powder XRD patterns of the resulting products at RT. Except for several minor peaks due to metal Fe and $Ca(OH_2)/Ca(OD_2)$ phases (< 5 wt%), all the peaks could be indexed to a tetragonal ZrCuSiAs-type[18] structure (space group:*P4/nmm*) with lattice constants $a = 0.3878$ and $c = 0.8260$ nm for CaFeAsH and $a = 0.3876$ and $c = 0.8257$ nm for CaFeAsD.[44] The differences in the lattice constants between the hydride and the deuteride versions were less than 0.05%. Rietveld analysis indicates that the observed XRD pattern is well explained by assuming a model structure composed of alternate layers of FeAs and CaH (CaD). However, the site position and occupancy of hydrogen cannot be determined by XRD because the x-ray atomic scattering factor of H^-/D^- is too small.

As shown in Fig. 1(b), weight loss involving the emission of the H_2 molecule was observed from 200 °C to 600 °C. The TG-MS measurement continued to 800 °C, where the sample decomposed into a mixture of $CaFe_2As_2$, FeAs, and unknown phases probably consisting of Ca with O_2, N_2, and/or H_2O gas from the He gas flow. The amount of released H_2 was estimated to be 3.08 mmol/g from the integration of the mass peak $m/z = 2$. This quantity was almost equal to that expected for the decomposition of CaFeAsH($2CaFeAsH \rightarrow Ca + CaFe_2As_2 + H_2\uparrow$, 2.91 mmol/g).

Since the coherent neutron scattering cross section of deuterium (5.592 b) is comparable to that of Ca (2.78), Fe (11.22), or As (5.44),[45] the atomic position and site occupancy of deuterium can be determined by NPD. Figure 1(c) shows NPD patterns observed at RT and 10 K. Rietveld analyses revealed that the anion site in the block layer is occupied by deuterium, with the site occupancy of 0.935.[44] Taking the isotopic purity of the $LiAlD_4$ and the inclusion of hydrogen from other starting materials into account, we conclude that the remaining fraction (0.065) of the anion site is primarily occupied by hydrogen. The NPD pattern observed at 10 K was attributed to an orthorhombic phase, space group: *Cmma*, $a = 0.549\ 213(16)$, $b = 0.545\ 660(16)$, and $c = 0.821\ 154(24)$ nm. This crystal symmetry change is the same as in other 1111-type iron arsenides with tetragonal to orthorhombic transitions reported in the range of 120–180 K. High-pressure synthesis appears to be essential for the formation of CaFeAsH because no such phase could be prepared at ambient pressures.

Figure 2(a) shows the temperature dependence of dc electrical resistivity (ρ) in CaFeAsH and CaFeAsD measured from 300 to 2 K. Both samples exhibit sudden decreases at ∼100 K (T_{anom}). This anomaly has also been observed in 1111- and 122-type iron arsenides and has been attributed to a tetragonal to orthorhombic transition.

Figure 2(b) shows the calculated total DOS and PDOS of CaFeAsH. The total energy was minimized with respect to both the coordinates of all atoms and the lattice parameters. Then, the stripe-type antiferromagnetic ordering of the Fe spins, commonly observed for 1111-type Fe arsenides below T_{anom}, was obtained as the most stable magnetic structure. Total DOS and Fe PDOS profiles revealed the semimetallic nature of CaFeAsH, with Fe 3*d* up-spin and down-spin bands overlapped at the Fermi level ($E = 0$). Hydrogen 1*s* levels were located

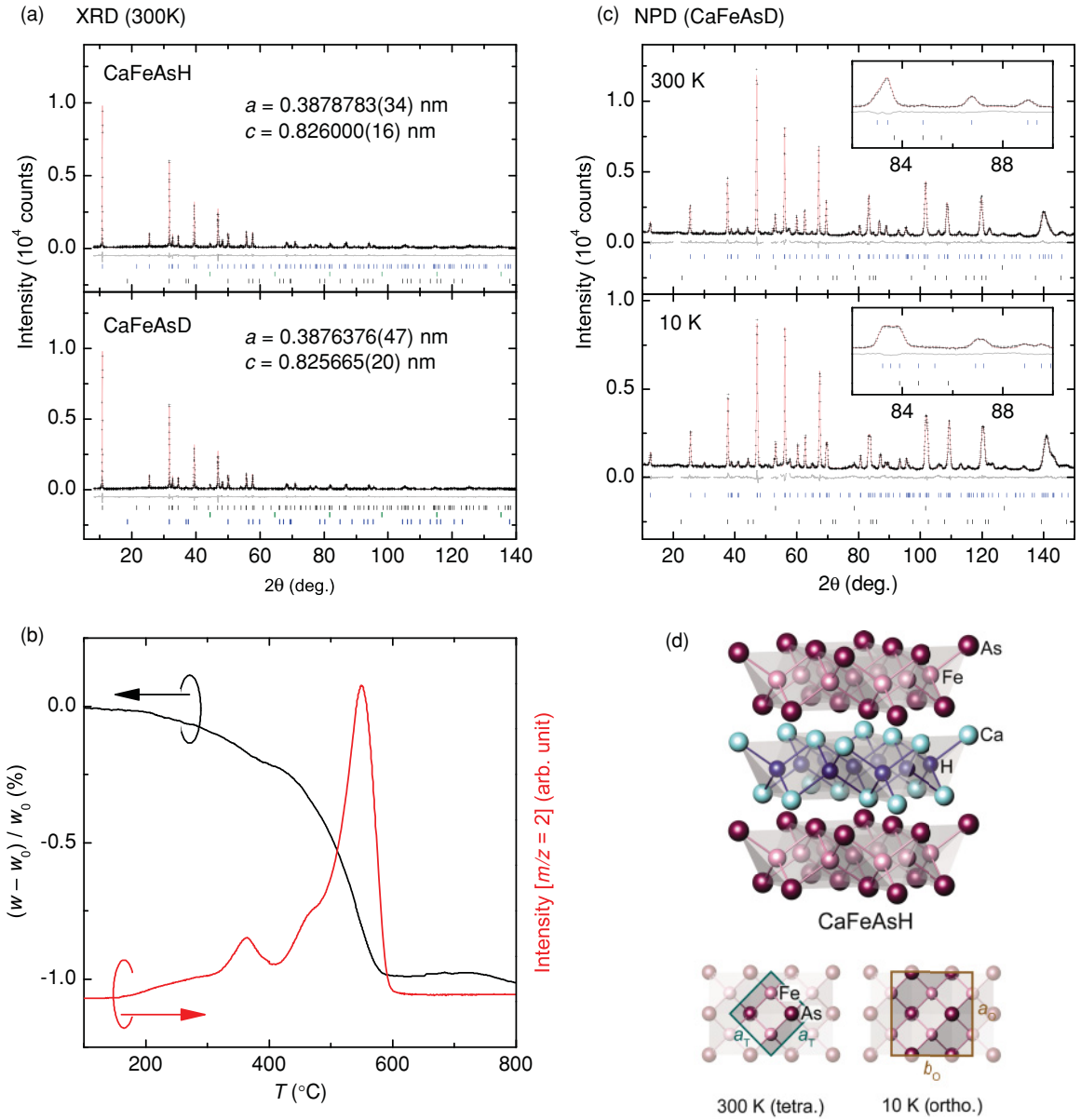

FIG. 1. (Color online) (a) Powder XRD patterns of CaFeAsH and CaFeAsD at room temperature (RT). (b) TG-MS ($m/z = 2$ corresponds to the H_2 molecule) profiles of CaFeAsH. Weight loss due the decomposition of the sample with hydrogen emission was observed from 200 °C to 600 °C. Hydrogen concentration was estimated to be 1.05 molecules per unit cell by integration of the MS trace curve. (c) NPD pattern of CaFeAsD observed at 300 and 10 K. (d) Crystal structure of CaFeAsH at 300 K (tetragonal) and 10 K (orthorhombic).

at ∼2 eV below the Fermi level and were fully occupied. It is evident from these results that hydrogen is incorporated as H^- ($1s^2$) in CaFeAsH. This finding is consistent with the similarities in the ρ-T curves of CaFeAsH and CaFeAsF, indicating that the replacement of F sites with H^- ions does not seriously affect the electronic structure of the FeAs conduction layer.

Based on the similarity of the charge and size of the hydride and fluorine ion, the formation of the solid solution $CaFeAsF_{1-x}H_x$ was expected. Figure 2(c) shows the lattice parameters a and c as a function of x. The value of x in the resulting $CaFeAsF_{1-x}H_x$ was evaluated by TG-MS measurement. While the lattice parameter a was almost independent of x, the value of c was proportional to x, indicating that the geometry of the $CaF_{1-x}H_x$ layer is determined by the weighted average of the ionic radius of F^- (r_F) and H^- (r_H). From the F-Ca distance ($r_F + r_{Ca} = 233.7$ pm) and the H-Ca bond length ($r_H + r_{Ca} = 230.2$ pm) evaluated from Rietveld analysis, the ionic radius of H^- was estimated for 1111-type iron arsenides. On the assumption that an F^- coordinated by four Ca^{2+} ions retains Shannon's ionic radius ($r_F = 131$ pm),[46] then, the ionic radius of Ca^{2+} was calculated to be 102.7 pm. The radius of H^- calculated from the H-Ca bond length (230.2 pm) in CaFeAsH is 127.5 pm, which is smaller than that of F^- by 2.8%.

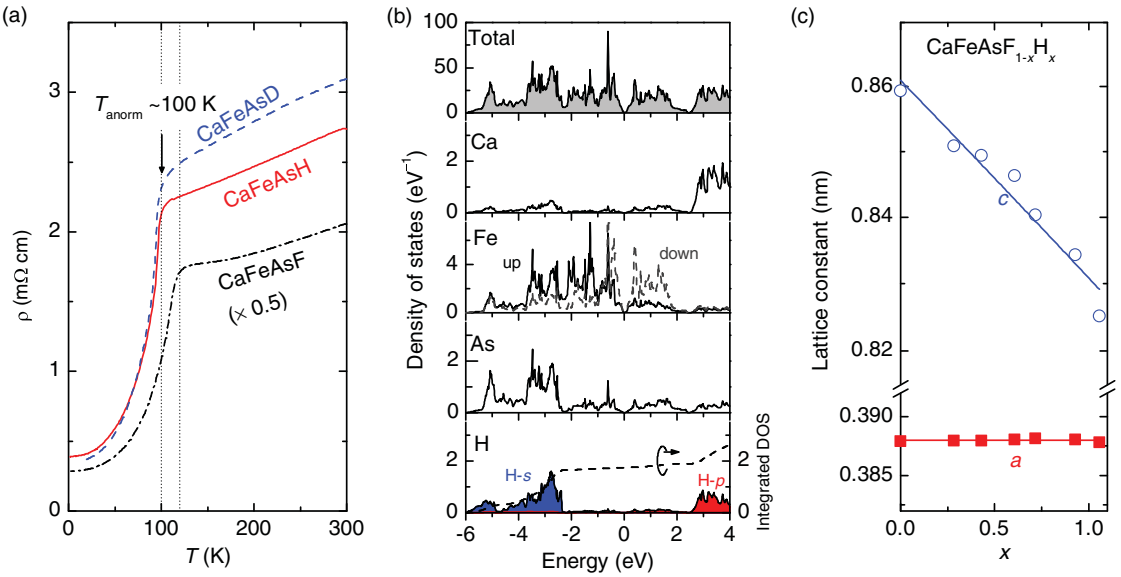

FIG. 2. (Color online) (a) ρ-T profile of CaFeAsH and CaFeAsD compared with CaFeAsF. (b) Total DOS and atomic projected density of states (PDOS) of CaFeAsH obtained by density functional calculation using the VASP code. The origin was set at the Fermi level. (c) Variation of lattice constants (a, c) as a function of x in the solid solution $CaFeAsF_{1-x}H_x$. Hydrogen content (x) was estimated by the TG-MS method.

Chevalier *et al.*[47] reported the synthesis of 1111-type hydrides Ln*MX*H (*M* = Mn, Fe, and Co; *X* = Si and Ge). These crystals, with stacks of alternating LnH hydride layers and *MX* layers, were made by hydrogen insertion onto CeFeSi-type[48] Ln*MX*. In contrast, the present high-pressure synthesis using hydrides does not require the precursor.

Then, the hydrogen-substitution technique was applied to electron doping in SmFeAsO. Figure 3(a) shows

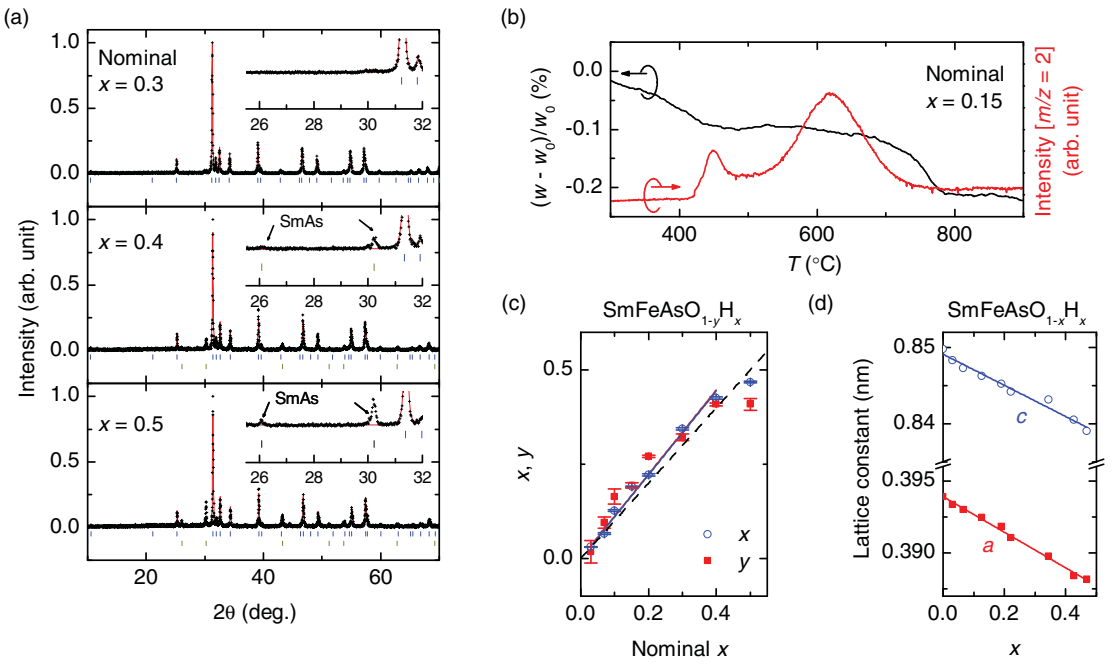

FIG. 3. (Color online) Structural and chemical composition data on $SmFeAsO_{1-x}H_x$. (a) Powder XRD patterns of $SmFeAsO_{1-x}H_x$ (nominal $x = 0.3$, 0.4, and 0.5). Insets show close-up views. (b) TG-MS ($m/z = 2$) profiles with nominal $x = 0.15$. H_2 gas emission associated with weight loss was observed from 400 °C to 800 °C. (c) Oxygen deficiency content determined by EPMA measurement (y) and hydrogen content estimated by the TG-MS method (x) in $SmFeAsO_{1-y}H_x$ as a function of nominal x in the starting mixture. The measured x is almost equal to y and nominal x, indicating the deficiency of the oxygen site is wholly compensated by the occupation of hydrogen. (d) Lattice constants (a and c) as a function of x.

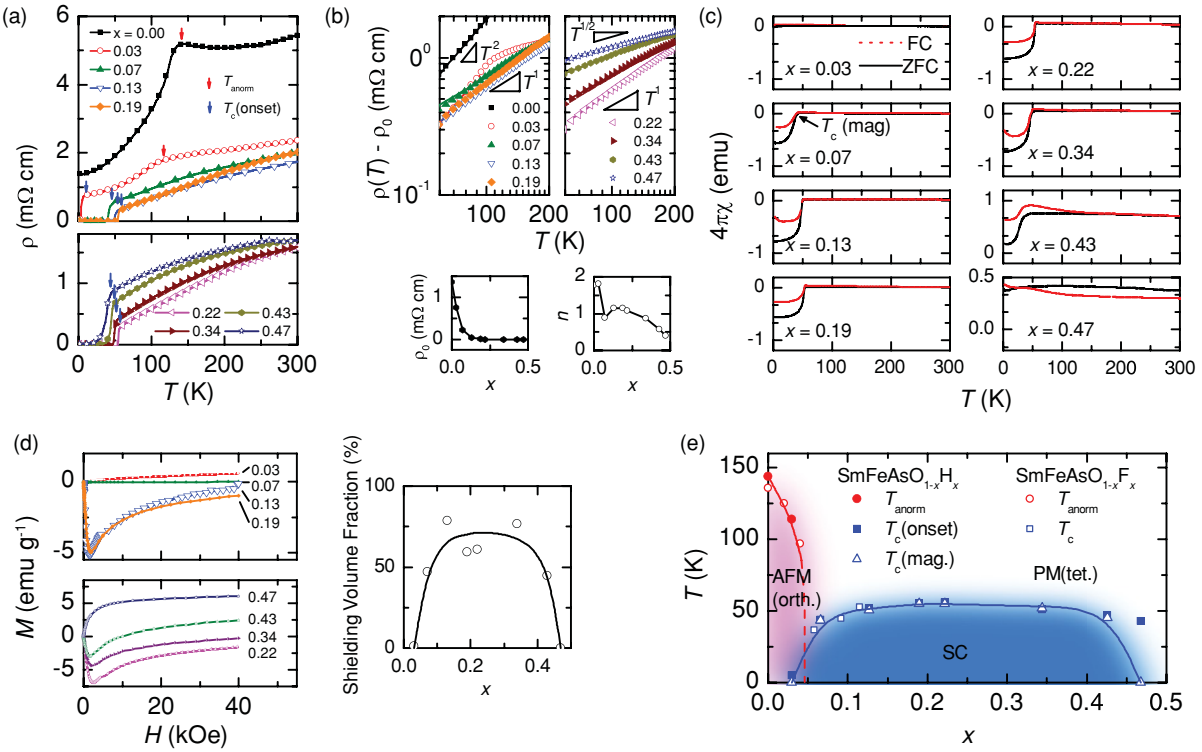

FIG. 4. (Color online) Electrical and magnetic properties. (a) ρ-T profiles of $SmFeAsO_{1-x}H_x$ in underdoped (left, $x = 0.0$–0.19) and overdoped states (right, $x = 0.22$–0.47). (b) Log $[\rho(T) - \rho_0]$ vs log T plots for data on the nonsuperconducting region, where ρ_0 is the residual component of resistivity obtained from fitting (see text). Lower parts show ρ_0 and the exponent residual resistivity n as a function of x. (c) ZFC and FC $4\pi\chi$-T curves measured under the magnetic field (H) of 10 Oe. (d) Magnetization (M) vs H curves and shielding volume fraction vs x plot at 2 K. (e) x-T diagram of $SmFeAsO_{1-x}H_x$ superimposed by that of $SmFeAsO_{1-x}F_x$.[33]

representative powder XRD patterns of $SmFeAsO_{1-x}H_x$ (nominal x values in starting mixtures are 0.3, 0.4, and 0.5). When nominal x exceeds ~0.4, the SmAs phase begins to segregate, implying the actual hydrogen content (x) is lower than the nominal x. Figure 3(b) shows the TG-MS profile ($m/z = 2$) of $SmFeAsO_{1-x}H_x$ with nominal $x = 0.15$. Hydrogen incorporated in $SmFeAsO_{1-x}H_x$ was released between 400 °C and 800 °C. The shape of the emission curve is close to that of $CaFeAsF_{1-x}H_x$. Figure 3(c) compares the hydrogen content (x) and the deficient amount of oxygen (y) in prepared samples per chemical formula ($SmFeAsO_1 - yH_x$) as a function of nominal x in the starting mixture. The former value was determined by TG-MS, and the latter was measured with EPMA. For nominal $x \leqslant 0.4$, the hydrogen content agrees with y and the nominal x, indicating the oxygen site (O^{2-}) was successfully substituted with hydrogen (H^-). Figure 3(d) shows the variation of lattice constants a and c of the $SmFeAsO_{1-x}H_x$ system. Same as $CaFeAsF_{1-x}H_x$, the decrease of c with x corresponds to the difference in ionic radii between O^{2-} (142 pm) and H^- (127.5 pm in $CaFeAsF_{1-x}H_x$). On the other hand, a of the $SmFeAsO_{1-x}H_x$ system apparently decreases with x. This result contrasts with the $CaFeAsF_{1-x}H_x$ system in which a is independent of x. It is likely to be a result of electron doping in the FeAs layer by H substitution ($O^{2-} = H^- + e^-$), i.e., the doped electrons occupy the bonding states (i.e., a hole pocket) of the FeAs layer and shorten the intralayer Fe-Fe distance.

Figure 4(a) shows the temperature dependence of the electrical resistivity in $SmFeAsO_{1-x}H_x$. A sudden drop of resistivity due to superconductivity was observed for $x \geqslant 0.03$, and the maximum critical temperature T_c (onset) was 55 K at $x \sim 0.2$. As x increased over 0.2, T_c decreased, indicating the appearance of an overdoped region. To reveal the change in transport properties of the normal conducting state with hydrogen substitution, we examined the exponent n of $\rho(T) \sim T^n$ for each sample by fitting the data to $\rho(T) = \rho_0 + AT^n$ in the temperature range between T just above T_c and $T = 130$ K, where ρ_0 is the residual component of resistivity. Figure 4(b) shows the results; n decreases from 2 to 1 with x below the optimal substitution level ($x < 0.2$), while ρ_0 rapidly decreases to 0. The T^2 dependence to high temperature is characteristic for strongly correlated Fermi liquid systems in which electron-electron interaction dominates the scattering of the carriers.[49] T linear dependence at the optimal level indicates a non-Fermi liquid state was induced by electron doping via hydrogen substitution. Similar behaviors have also been observed in 122-type and some 1111-type iron arsenides.[50,51] On the contrary, n deceases to 0.5 in the overdoping region ($x > 0.2$). This is quite different from 122-type arsenide in which n again is close to ~2 in the overdoping region. Figure 4(c) shows magnetic susceptibility ($4\pi\chi$) vs T plots of $x = 0.03$–0.47 samples under ZFC and FC with a magnetic field of 10 Oe. The diamagnetism due to superconductivity was observed below T_c (mag) for $x = 0.07$–0.43. Shielding volume

fraction (SVF) of each sample was obtained from the gradient of the liner region in the magnetization (M) vs the field (H) plot observed at 2 K [Fig. 4(d)]. The SVF above 45% observed for $x = 0.07$–0.43 indicates the bulk superconductivity, whereas, the SVF in $x = 0.03$ and 0.47 samples is lower than 1%. Such a low SVF implies that the zero resistivity is due to the inhomogeneity of hydrogen concentration not bulk superconductivity. The sample of $x = 0.03$ shows both the sudden drop of resistivity due to superconducting transition ($T_c = 5$ K) and the ρ-T anomaly ($T_{anorm} = 114$ K) due to crystallographic transition accompanied with magnetic ordering of the Fe spins. Similar behavior has been observed in $SmFeAsO_{1-x}F_x$ around $x \sim 0.04$.[32] These data imply the coexistence of superconductivity and magnetic ordering in the limited x range near 0.03–0.04. While such coexistence has been confirmed in 122-type iron-arsenide superconductors,[26] it is hard to distinguish from the coexistence in systems with compositional disorder. Detailed experiments using an appropriate microprobe, such as μSR are required to clarify the intrinsic nature of this coexistence. Figure 4(e) shows the x-T diagram of $SmFeAsO_{1-x}H_x$ superimposed with that of $SmFeAsO_{1-x}F_x$ with the fluorine content x measured by EPMA as reported by Köhler and Behr[33] in which the T_c vs x plots of $SmFeAsO_{1-x}H_x$ and $SmFeAsO_{1-x}F_x$ overlap at $x < 0.15$, indicating that hydrogen gives indirect electron doping to the FeAs layer just like fluorine. While the solubility limit of fluorine in the oxygen site is restricted to less than 20% ($x = 0.2$),[33,34] hydrogen can reach 40%. The wider substitution range is useful for the optimization of the electron-doping level to induce superconductivity and to complete the electronic phase diagram, including the overdoped region.

IV. SUMMARY

The 1111-type $CaFeAsF_{1-x}H_x$ ($0 < x \leqslant 1$) and $SmFeAsO_{1-x}H_x$ ($0 < x \leqslant 0.4$) were synthesized by a high-pressure technique with an excess hydrogen source. Substitution of H^- into the F^- site in CaFeAsF was confirmed by NPD analysis and density functional calculations. The resulting $CaFeAsF_{1-x}H_x$ were nonsuperconducting with a ρ-T anomaly at ~100 K due to a tetragonal to orthorhombic transition commonly observed in AeFeAsF and LnFeAsO. In $SmFeAsO_{1-x}H_x$ ($0 < x \leqslant 0.4$), H^- substitution into the O^{2-} site supplies electrons to the FeAs layer, giving rise to superconductivity with an optimized T_c of 55 K. Further H^- substitution beyond the optimal level leads to a decrease in T_c up to $x = 0.4$. The present results suggest the hydrogen (H^-) substitution to the anion site is generally applicable for electron doping in 1111-type iron-arsenide superconductors.

ACKNOWLEDGMENTS

We thank Toshiyuki Atou and Osamu Fukunaga of the Tokyo Institute of Technology for their valuable discussions. This research is funded by the Japan Society for the Promotion of Science (JSPS) through the FIRST program, initiated by the CSTP.

*hosono@msl.titech.ac.jp

[1] Y. Kamihara, T. Watanabe, M. Hirano, and H. Hosono, J. Am. Chem. Soc. **130**, 3296 (2008).
[2] M. Rotter, M. Tegel, and D. Johrendt, Phys. Rev. Lett. **101**, 107006 (2008).
[3] C. Gen-Fu, L. Zheng, L. Gang, H. Wan-Zheng, D. Jing, Z. Jun, Z. Xiao-Dong, Z. Ping, W. Nan-Lin, and L. Jian-Lin, Chin. Phys. Lett. **25**, 3403 (2008).
[4] G. Wu, H. Chen, T. Wu, Y. L. Xie, Y. J. Yan, R. H. Liu, X. F. Wang, J. J. Ying, and X. H. Chen, J. Phys.: Condens. Matter **20**, 422201 (2008).
[5] F. Hsu, J. Luo, K. Yeh, T. Chen, T. Huang, P. M. Wu, Y. Lee, Y. Huang, Y. Chu, D. Yan, and M. Wu, Proc. Natl. Acad. Sci. USA **105**, 14262 (2008).
[6] X. Wang, Q. Liu, Y. Lv, W. Gao, L. Yang, R. Yu, F. Li, and C. Jin, Solid State Commun. **148**, 538 (2008).
[7] H. Ogino, Y. Matsumura, Y. Katsura, K. Ushiyama, S. Horii, K. Kishio, and J. Shimoyama, Supercond. Sci. Technol. **22**, 075008 (2009).
[8] X. Zhu, F. Han, G. Mu, P. Cheng, B. Shen, B. Zeng, and H. Wen, Sci. China, Ser. G **52**, 1876 (2010).
[9] X. Zhu, F. Han, G. Mu, P. Cheng, B. Shen, B. Zeng, and H. H. Wen, Phys. Rev. B **79**, 220512 (2009).
[10] G. F. Chen, T. Xia, H. X. Yang, J. Q. Li, P. Zheng, J. L. Luo, and N. L. Wang, Supercond. Sci. Technol. **22**, 072001 (2009).
[11] J. Guo, S. Jin, G. Wang, S. Wang, K. Zhu, T. Zhou, M. He, and X. Chen, Phys. Rev. B **82**, 180520 (2010).
[12] H. Takahashi, K. Igawa, K. Arii, Y. Kamihara, M. Hirano, and H. Hosono, Nature (London) **453**, 376 (2008).
[13] G. F. Chen, Z. Li, D. Wu, G. Li, W. Z. Hu, J. Dong, P. Zheng, J. L. Luo, and N. L. Wang, Phys. Rev. Lett. **100**, 247002 (2008).
[14] Z. A. Ren, J. Yang, W. Lu, W. Yi, G. C. Che, X. L. Dong, L. L. Sun, and Z. X. Zhao, Mater. Res. Innovations **12**, 105 (2008).
[15] Z. Ren, J. Yang, W. Lu, W. Yi, X. Shen, Z. Li, G. Che, X. Dong, L. Sun, F. Zhou, and Z. Zhao, Europhys. Lett. **82**, 57002 (2008).
[16] X. H. Chen, T. Wu, G. Wu, R. H. Liu, H. Chen, and D. F. Fang, Nature (London) **453**, 761 (2008).
[17] R. Zhi-An, L. Wei, Y. Jie, Y. Wei, S. Xiao-Li, Zheng-Cai, C. Guang-Can, D. Xiao-Li, S. Li-Ling, Z. Fang, and Z. Zhong-Xian, Chin. Phys. Lett. **25**, 2215 (2008).
[18] R. Pöttgen and D. Johrendt, Z. Naturforsch., B: Chem. Sci. **63**, 1135 (2008).
[19] Z. Ren, G. Che, X. Dong, J. Yang, W. Lu, W. Yi, X. Shen, Z. Li, L. Sun, F. Zhou, and Z. Zhao, Europhys. Lett. **83**, 17002 (2008).
[20] H. Kito, H. Eisaki, and A. Iyo, J. Phys. Soc. Jpn. **77**, 063707 (2008).
[21] K. Miyazawa, K. Kihou, P. M. Shirage, C. Lee, H. Kito, H. Eisaki, and A. Iyo, J. Phys. Soc. Jpn. **78**, 034712 (2009).
[22] A. S. Sefat, A. Huq, M. A. McGuire, R. Jin, B. C. Sales, D. Mandrus, L. M. D. Cranswick, P. W. Stephens, and K. H. Stone, Phys. Rev. B **78**, 104505 (2008).

[23]C. Wang, Y. K. Li, Z. W. Zhu, S. Jiang, X. Lin, Y. K. Luo, S. Chi, L. J. Li, Z. Ren, M. He, H. Chen, Y. T. Wang, Q. Tao, G. H. Cao, and Z. A. Xu, Phys. Rev. B **79**, 054521 (2009).
[24]G. Cao, S. Jiang, X. Lin, C. Wang, Y. Li, Z. Ren, Q. Tao, C. Feng, J. Dai, Z. Xu, and F. C. Zhang, Phys. Rev. B **79**, 174505 (2009).
[25]Y. K. Li, X. Lin, T. Zhou, J. Q. Shen, Q. Tao, G. H. Cao, and Z. A. Xu, J. Phys.: Condens. Matter **21**, 355702 (2009).
[26]H. Chen, Y. Ren, Y. Qiu, W. Bao, R. H. Liu, G. Wu, T. Wu, Y. L. Xie, X. F. Wang, Q. Huang, and X. H. Chen, EPL **85**, 5 (2009).
[27]K. Miyazawa, K. Kihou, P. M. Shirage, C. Lee, H. Kito, H. Eisaki, and A. Iyo, J. Phys. Soc. Jpn. **78**, 034712 (2009).
[28]P. M. Shirage, K. Miyazawa, K. Kihou, H. Kito, Y. Yoshida, Y. Tanaka, H. Eisaki, and A. Iyo, Phys. Rev. Lett. **105**, 037004 (2010).
[29]K. Miyazawa, S. Ishida, K. Kihou, P. M. Shirage, M. Nakajima, C. H. Lee, H. Kito, Y. Tomioka, T. Ito, H. Eisaki, H. Yamashita, H. Mukuda, K. Tokiwa, S. Uchida, and A. Iyo, Appl. Phys. Lett. **96**, 072514 (2010).
[30]S. Matsuishi, Y. Inoue, T. Nomura, H. Yanagi, M. Hirano, and H. Hosono, J. Am. Chem. Soc. **130**, 14428 (2008).
[31]S. Matsuishi, Y. Inoue, T. Nomura, Y. Kamihara, M. Hirano, and H. Hosono, New J. Phys. **11**, 025012 (2009).
[32]Y. Kamihara, T. Nomura, M. Hirano, J. Eun Kim, K. Kato, M. Takata, Y. Kobayashi, S. Kitao, S. Higashitaniguchi, Y. Yoda, M. Seto, and H. Hosono, New J. Phys. **12**, 033005 (2010).
[33]A. Köhler and G. Behr, J. Supercond. Novel Magn. **22**, 565 (2009).
[34]G. Prando, P. Carretta, A. Rigamonti, S. Sanna, A. Palenzona, M. Putti, and M. Tropeano, Phys. Rev. B **81**, 100508 (2010).
[35]Y. Fukai and N. Okuma, Jpn. J. Appl. Phys. **32**, L1256 (1993).
[36]Y. Fukai and N. Okuma, Phys. Rev. Lett. **73**, 1640 (1994).
[37]TOPAS (Bruker AXS GmbH, Karlsruhe, Germany, 2009).
[38]F. Izumi and K. Momma, Solid State Phenomena **130**, 15 (2007).
[39]J. P. Perdew, K. Burke, and M. Ernzerhof, Phys. Rev. Lett. **77**, 3865 (1996); **78**, 1396(E) (1997).
[40]P. E. Blöchl, Phys. Rev. B **50**, 17953 (1994).
[41]G. Kresse and J. Furthmüller, Phys. Rev. B **54**, 11169 (1996).
[42]T. Nomura, S. W. Kim, Y. Kamihara, M. Hirano, P. V. Sushko, K. Kato, M. Takata, A. L. Shluger, and H. Hosono, Supercond. Sci. Technol. **21**, 125028 (2008).
[43]P. V. Sushko, A. L. Shluger, M. Hirano, and H. Hosono, Phys. Rev. B **78**, 172508 (2008).
[44]See Supplemental Material at http://link.aps.org/supplemental/10.1103/PhysRevB.84.024521 for CIF files containing crystallographic information of CaFeAsH(D) crystals obtained by Rietveld refinements of XRD and NPD patterns.
[45]V. F. Sears, Neutron News **3**, 26 (1992).
[46]R. D. Shannon, Acta Crystallogr., Sect. A: Cryst. Phys., Diffr., Theor. Gen. Crystallogr. **32**, 751 (1976).
[47]B. Chevalier, M. Pasturel, J. Bobet, and O. Isnard, Solid State Commun. **134**, 529 (2005).
[48]O. I. Bodak, E. I. Gladyshevskii, and P. I. Kripyakevich, J. Struct. Chem. **11**, 283 (1970).
[49]M. Imada, A. Fujimori, and Y. Tokura, Rev. Mod. Phys. **70**, 1039 (1998).
[50]S. Kasahara, T. Shibauchi, K. Hashimoto, K. Ikada, S. Tonegawa, R. Okazaki, H. Shishido, H. Ikeda, H. Takeya, K. Hirata, T. Terashima, and Y. Matsuda, Phys. Rev. B **81**, 184519 (2010).
[51]S. Ishida, M. Nakajima, Y. Tomioka, T. Ito, K. Miyazawa, H. Kito, C. H. Lee, M. Ishikado, S. Shamoto, A. Iyo, H. Eisaki, K. M. Kojima, and S. Uchida, Phys. Rev. B **81**, 094515 (2010).